

# Computational methods in the physical interpretation of Robinson-Trautman spacetimes

Daniel A. Prager and Anthony W.C. Lun  
*Mathematics Department, Monash University,  
Clayton, Vic 3168, Australia*

## Abstract

In the Relaxed Bondi-Sachs coordinates devised by Fletcher and Lun [1] one of the field equations may be interpreted as a generalisation of the Robinson-Trautman equation. Accordingly, by extensively investigating the Robinson-Trautman spacetimes [2] (whose evolutions are governed by the Robinson-Trautman equation) we are laying the groundwork for more general evolutions in the characteristic setting of Numerical Relativity.

We have devised numerical schemes which successfully evolve the axisymmetric Robinson-Trautman equation using two distinct methods: finite differences and a spectral method (the latter proves superior). We are presently attempting to match a dust interior to the vacuum exterior. The first step in the matching is to determine the history of the collapsing surface by following eventually radial time-like geodesics backwards in retarded time from near the event horizon. We present preliminary results on the history of the shell of test particles. In general, as the test particles proceed backwards they acquire a tangential component to their motion.

## 1. Introduction

The vacuum Robinson-Trautman spacetimes are a class of distorted black holes which possess a future event horizon and a past apparent horizon [3]. As they evolve these objects radiate energy in the form of purely outgoing gravitational waves and settle down to the Schwarzschild solution in the limit of large retarded time [4]. Their evolution is governed by a single field equation, the Robinson-Trautman equation.

With the exception of the steady state (the Schwarzschild solution) and Minkowski spacetime in Newman-Unti coordinates no exact regular solutions to the Robinson-Trautman equation are known. However, many strong results about the global behaviour of this equation have been established: Chruściel [5] proved that solutions exist for quite general initial conditions; Tod [6] demonstrated uniqueness; in the limit of large retarded time the vacuum Robinson-Trautman spacetime settles down to the Schwarzschild solution; several conserved and monotonically decreasing (Lyapunov) quantities are known, the most readily interpretable of which is the Bondi mass. It gives a measure of the total mass-energy on each null-slice.

Since at large retarded times the vacuum Robinson-Trautman spacetimes settle down to Schwarzschild, it seems reasonable that generalisations to some of the classic matchings

of a Schwarzschild exterior to various matter interiors may be possible. The latter part of this paper describes preliminary work towards matching the vacuum Robinson-Trautman exterior to a dust interior. If successful, this matching would constitute a direct generalisation of the Oppenheimer-Snyder solution, and would correspond to that solution in the limit of large retarded time. This matching would constitute a numerical solution, rather than an exact solution.

## 2. Numerical evolution of the Robinson-Trautman exterior

The line element of the vacuum Robinson-Trautman equation with  $(+, -, -, -)$  signature can be written

$$ds^2 = 2Hdu^2 + 2dudr - \frac{r^2}{f^2}d\Omega^2 \quad (1)$$

where  $u$  is retarded time and  $r$  is a radial coordinate along the light-cone (i.e.  $\partial_r$  is a null vector).  $2H = -2r\frac{f_u}{f} + K - \frac{2m}{r}$ ,  $f = f(u, \Omega) > 0$ ,  $d\Omega^2$  is the line-element of the unit 2-sphere, and the constant  $m$  is the mass of the steady-state solution.  $K$  denotes the Gaussian curvature of the topological 2-sphere with line element  $\frac{1}{f^2}d\Omega^2$ , given by

$$K(u, \Omega) = f^2 (\Delta_0(\ln f) + 1) \quad (2)$$

where  $\Delta_0$  is the standard Laplacian operator on the unit 2-sphere. The only field equation (the Robinson-Trautman equation) is given by

$$f_{,u} = -\frac{f^3}{12m}\Delta_0 K \quad (3)$$

with initial condition  $f(0, \Omega) = f_0(\Omega) > 0$ . The Robinson-Trautman equation is a fourth-order, non-linear, parabolic equation.

In an earlier paper [7] the authors described an algorithm for the accurate and efficient numerical evolution of the axisymmetric Robinson-Trautman equation by a spectral method. (This approach refined earlier numerical work of Singleton [8] based on finite differences.) The full non-axisymmetric case should not present any great difficulties, at least in principle, but calls for substantially greater computing resources.

A number of strong theoretical results which describe various aspects of the global behaviour of the Robinson-Trautman equation have been established. For the purposes of numerical studies the most significant are the conservation of surface area

$$A(u) = \int_{S^2} f(u, \Omega)^{-2} d\Omega^2 = 4\pi \quad (4)$$

and the monotonic decrease of the Bondi mass

$$M_B(u) = \frac{m}{4\pi} \int_{S^2} f(u, \Omega)^{-3} d\Omega^2 \quad (5)$$

The surface area is not exactly conserved in computations, but its change gives a useful measure of error. The Bondi mass is important for physical interpretation.

One feature of the Robinson-Trautman equation, arising from residual coordinate freedom in the description of the two-sphere, is the non-uniqueness of the representation of  $f$ . For instance, the final state, which always corresponds to the Schwarzschild solution, consists of a superposition of the zero and first harmonics, i.e.

$$f_\infty(\theta, \phi) = A + B \cos \theta + C \sin \theta \cos \phi + D \sin \theta \sin \phi \quad (6)$$

with  $A, B, C$  and  $D$  constants subject to a normalisation constraint to ensure that surface area is  $4\pi$ , but otherwise unrestricted. In general it is not possible, given arbitrary initial data, to predict the final state; it is necessary to run a numerical evolution. However, the authors, in collaboration with E W-M Chow [7], have devised a procedure which makes it possible to rescale arbitrary initial data so that the final state consists purely of the zero harmonic (i.e.  $A = 1, B = C = D = 0$ ). In the axisymmetric case, where  $C = D = 0$  automatically from the symmetry, the appropriate transformation of the initial data is given by

$$\tilde{f}_0(\tilde{z}) = (A - B\tilde{z})f_0\left[\frac{A - B\tilde{z}}{B\tilde{z} - A}\right]$$

where  $z = \cos \theta$ . To implement this scheme it is appropriate to evolve the data numerically twice. The first run determines the end-state of the original data, yielding  $A$  and  $B$ . We could now, in theory, carry out a rescaling at every time-step. However, it is preferable to re-do the evolution with the rescaled data. Discrepancy from the expected  $\tilde{f}_\infty(\tilde{z}) = 1$  steady-state solution is an excellent measure of error.

Consider, for example, the axisymmetric initial data

$$f_0(z) = \alpha(1 + 0.3z + 0.3z^2 - 0.2z^3 - 0.2z^4 - 0.2z^5)$$

where  $\alpha$  is a normalisation constraint which is scaled to ensure that  $A(0) = 4\pi$ .  $m$  is set to  $1/12$ . Numerical evolution shows that the steady state (to four decimal places) is

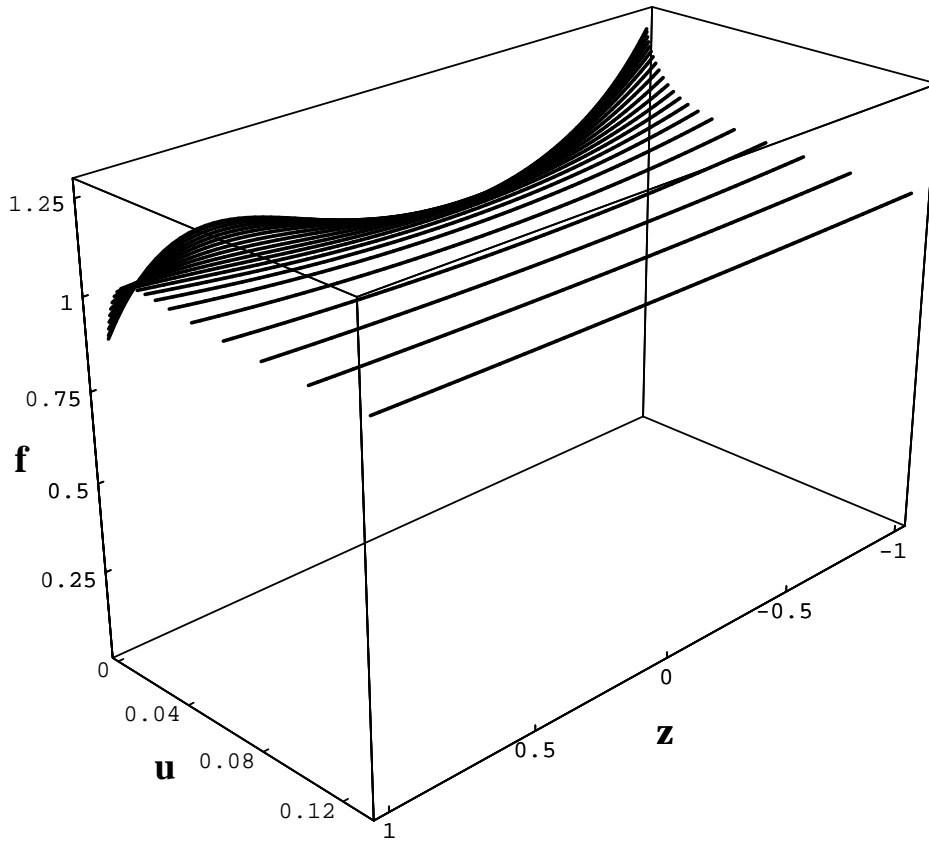
$$f_\infty(z) = 1.0035 + 0.0842z$$

Following rescaling of initial data, and re-evolving, the new final state is given by

$$\tilde{f}_\infty(\tilde{z}) = 1 + 1.3 \cdot 10^{-10} \tilde{z}$$

In these calculations 30 spectral modes were used and each evolution took 20 seconds on a DEC Alpha 3000. The error in surface area was  $7.6 \cdot 10^{-10}$ . Figure (1) shows every 10th time-step of the second evolution. Figure (2) shows the monotonic decay of the Bondi mass.

Table (1) compares the discrepancy between the final state (following re-scaling) and 1 for several different grid resolutions, for both spectral methods and finite differences.

Figure 1: Evolution of the conformal factor,  $f(u, z)$ 

Spectral Modes	Error	Finite Difference Points
10	$3 \cdot 10^{-5}$	100
	$6 \cdot 10^{-6}$	200
	$1.3 \cdot 10^{-6}$	400
	$10^{-6}$	
15	$1.8 \cdot 10^{-9}$	
20	$1.3 \cdot 10^{-10}$	
30	$1.3 \cdot 10^{-10}$	

Table 1: Comparison of spectral and finite difference evolutions

While the finite difference scheme converges quadratically, the spectral scheme converges exponentially.

It is worth noting that with a grid resolution of 400 finite difference modes round-off error begins to effect the numerical results. For instance, the numerical estimate of the Bondi mass is found to increase slightly at large retarded times.

### Bondi mass

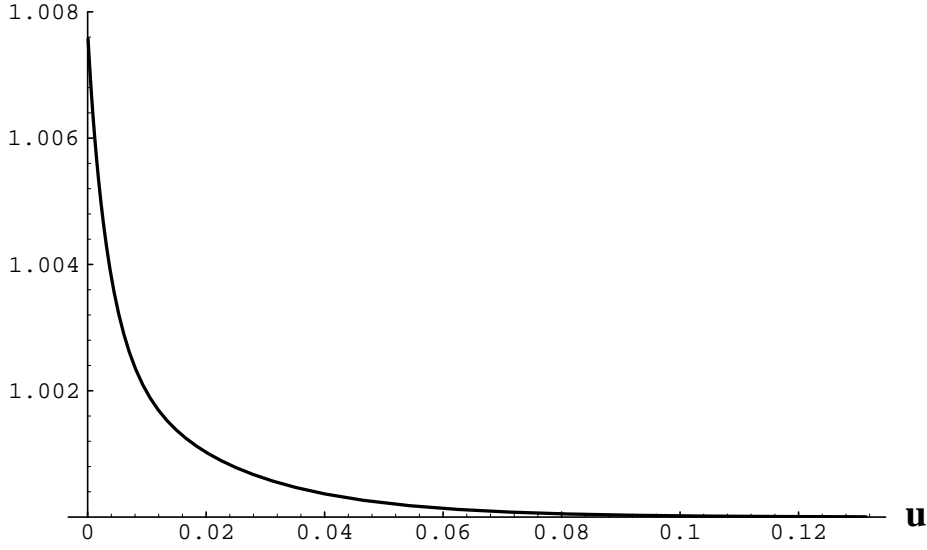


Figure 2: Decay of the scaled Bondi mass,  $M_B(u)/m$

## 3. Timelike geodesics

### 3.1 The geodesic equations

We derive the geodesic equations for the axisymmetric case by extremising the Lagrangian

$$\mathcal{L} = 2H\dot{u}^2 + 2\dot{u}\dot{r} - \frac{r^2}{f^2(1-z^2)}\dot{z}^2 \quad (7)$$

where  $\dot{x}^i := \frac{dx^i}{d\tau}$ ,  $\tau$  is proper time along the geodesic, and  $z = \cos \theta$ . The Euler-Lagrange equations,  $\frac{d}{d\tau}(\frac{\partial \mathcal{L}}{\partial \dot{x}^i}) = \frac{\partial \mathcal{L}}{\partial x^i}$ , yield

$$2H\ddot{u} + \ddot{r} = -H_{,u}\dot{u} - 2H_{,r}\dot{r} - 2H_{,z}\dot{z} + \frac{r^2 f_{,u}}{f^3(1-z^2)}\dot{z}^2 \quad (8)$$

$$\ddot{u} = H_{,r}\dot{u}^2 - \frac{r}{f^2(1-z^2)}\dot{z}^2 \quad (9)$$

$$\frac{d}{d\tau}\left(\frac{r^2\dot{z}}{f^2(1-z^2)}\right) = -H_{,z}\dot{u}^2 + \frac{r^2 z}{f^2(1-z^2)^2}\dot{z}^2 \quad (10)$$

Since the geodesics are timelike

$$1 = g_{\mu\nu}\dot{x}^\mu\dot{x}^\nu = 2H\dot{u}^2 + 2\dot{u}\dot{r} - \frac{r^2}{f^2(1-z^2)}\dot{z}^2 \quad (11)$$

The numerically generated spacetime is parameterised in terms of retarded time so it is necessary to re-parameterise the equations. The  $\tau$ -derivatives are rewritten in terms of  $u$ , by means of the transformations

$$\dot{x}^i = \frac{(x^i)'}{\tau'} \quad (12)$$

$$\ddot{x}^i = \frac{(x^i)''\tau' - (x^i)'\tau''}{(\tau')^3} \quad (13)$$

where  $(x^i)' := \frac{dx^i}{du}$ . We also introduce a new variable

$$\left[ \frac{d\sigma}{du} \right] := \frac{r}{f\sqrt{1-z^2}} \frac{dz}{du} \quad (14)$$

to help simplify the structure of the resulting system of equations. The reorganised system eliminates one equation, depends on  $u$ , and has been reduced to first-order. The dependent variables are emphasised by enclosure in square brackets.

$$\frac{d}{du}[r] = \frac{\left[ \frac{d\sigma}{du} \right]^2 + \left[ \frac{d\tau}{du} \right]^2}{2} - H \quad (15)$$

$$\frac{d}{du}[z] = \frac{f\sqrt{1-z^2}}{[r]} \left[ \frac{d\sigma}{du} \right] \quad (16)$$

$$\frac{d}{du} \left[ \frac{d\tau}{du} \right] = \left( -H_{,r} + \frac{\left[ \frac{d\sigma}{du} \right]^2}{[r]} \right) \left[ \frac{d\tau}{du} \right] \quad (17)$$

$$\begin{aligned} \frac{d}{du} \left[ \frac{d\sigma}{du} \right] &= \left( -H_{,r} + \frac{H}{[r]} + \frac{f_{,u}}{f} + \frac{\left[ \frac{d\sigma}{du} \right]^2 - \left[ \frac{d\tau}{du} \right]^2}{2[r]} \right) \left[ \frac{d\sigma}{du} \right] \\ &\quad - \frac{f}{r\sqrt{1-z^2}} H_{,z} \end{aligned} \quad (18)$$

Equation (15) was obtained from equation (7) and the timelike condition (11). Equation (16) is a rearrangement of the definition (14). Equation (17) was derived from equation (9). Equation (18) was derived from equations (10) and (15).

We note that equation (8) was not needed to derive equations (15) – (18). Use of equation (8) would have led to a lengthy expression for  $\frac{d}{du} \left( \frac{d\tau}{du} \right)$ .

It is evident from the form of equation (17) that  $\left[ \frac{d\tau}{du} \right]$  cannot change sign. To measure the passage of proper time along each geodesic we supplement equations (15) – (18) with an additional equation:

$$\frac{d}{du}[\tau] = \left[ \frac{d\tau}{du} \right] \quad (19)$$

### 3.2 Final conditions

The Oppenheimer-Snyder solution consists of a collapsing spherically symmetric dust cloud with Schwarzschild exterior. If we were to extrapolate this solution backwards in time the dust would come to rest at infinite radius. Therefore, having evolved the Robinson-Trautman exterior to a large value of  $u$ , where it has effectively reached the Schwarzschild steady-state, we now wish to send dust particles which correspond to surface particles on the Oppenheimer-Snyder dust cloud flying backwards in time along timelike geodesics. The appropriate “final conditions” for such particles are given by

$$r = (2 + \epsilon)m \quad (20)$$

$$z \in (-1, 1) \quad (21)$$

$$\tau = 0 \quad (22)$$

$$\left[ \frac{d\tau}{du} \right] = 1 - \sqrt{\frac{2m}{r}} \quad (23)$$

$$\left[ \frac{d\sigma}{du} \right] = 0 \quad (24)$$

$\epsilon$  indicates how close to the event horizon the particles are when they commence their flight backwards. Since the usual coordinates of the Robinson-Trautman spacetime do not cover the interior of the black hole and exclude the event horizon, we should choose  $\epsilon > 0$ . Condition (21) indicates that representative particles from all latitudes may be included, and the choice that  $\tau$  be finally zero is arbitrary. Equation (23) specifies that the energy of particles would take them to rest at spatial infinity if they were moving through Schwarzschild spacetime. Equation (24) is due to eventual spherical symmetry.

### 3.3 A collapsing dust-cloud

Returning to our example, we may now integrate the geodesic equations using fourth-order Runge-Kutta integration, evaluating  $f$ ,  $H$  and their derivatives using the spectral solution to the Robinson-Trautman equation. We compare the motion of the dust particles with the surface particles in the Oppenheimer-Snyder dust-ball, for which

$$r(\tau) = \left( r(0)^{3/2} - 3\tau \sqrt{\frac{m}{2}} \right)^{\frac{2}{3}} \quad (25)$$

and  $z(\tau) = \text{const.}$  Figure 3 plots the radii of dust particles at points close to the north and south poles. The solid lines refer to the motion of dust particles released in the Robinson-Trautman spacetime with initial data as per the earlier example with  $\epsilon = 0.1$ . The dashed lines show the motion of corresponding Oppenheimer-Snyder particles. Figure 4 plots the motion of two non-polar particles.

Spherical symmetry prevents any angular motion in the Oppenheimer-Snyder solution, but in our example  $z$  changes with proper time (see Figure 5).

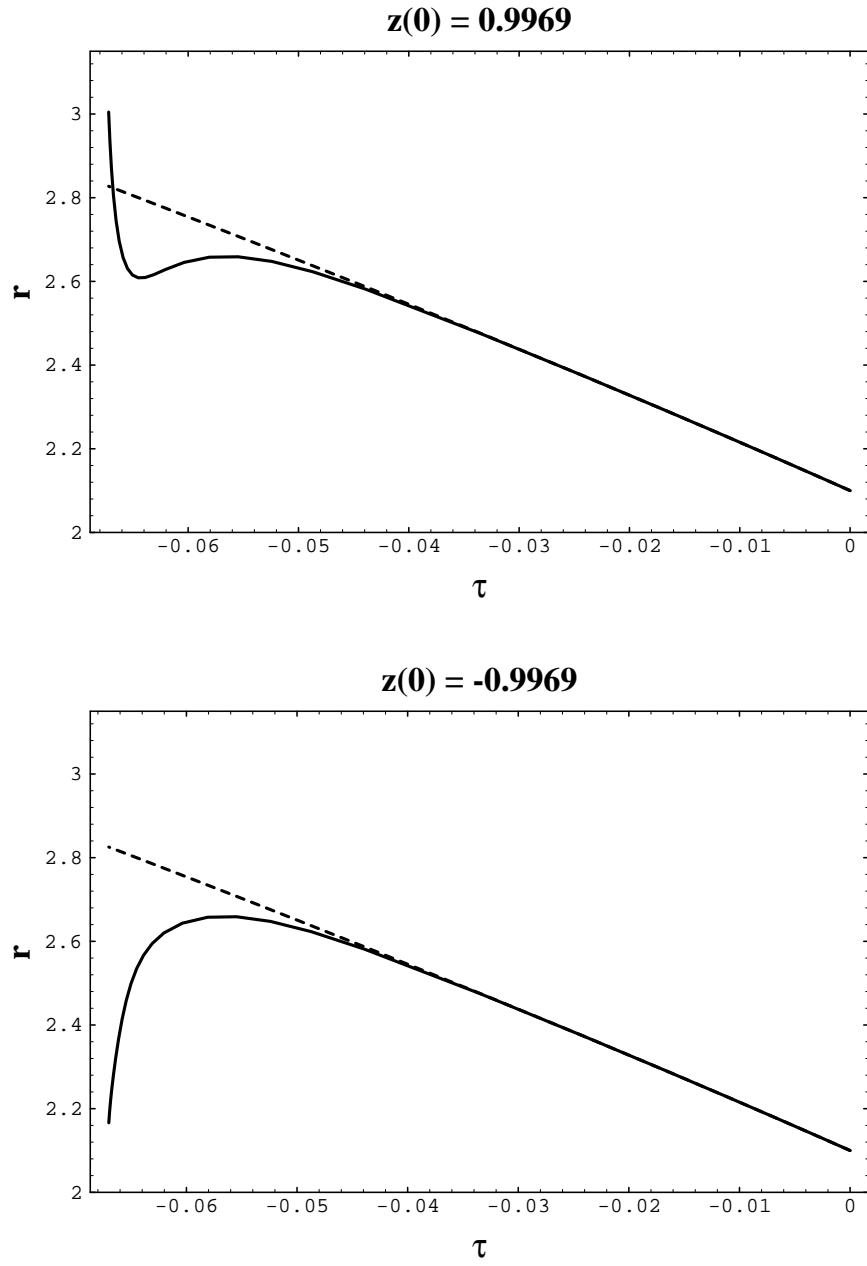


Figure 3: Radius of the dust cloud near the poles

Figure 6 contains a sequence of snapshots of the dust-cloud. The retarded time is the only candidate for a global time. Accordingly  $u$  is used to label the snapshots. The images are vertical slices of the dust-cloud through the poles — the axis of rotational symmetry runs up the page, through the centre of each image.



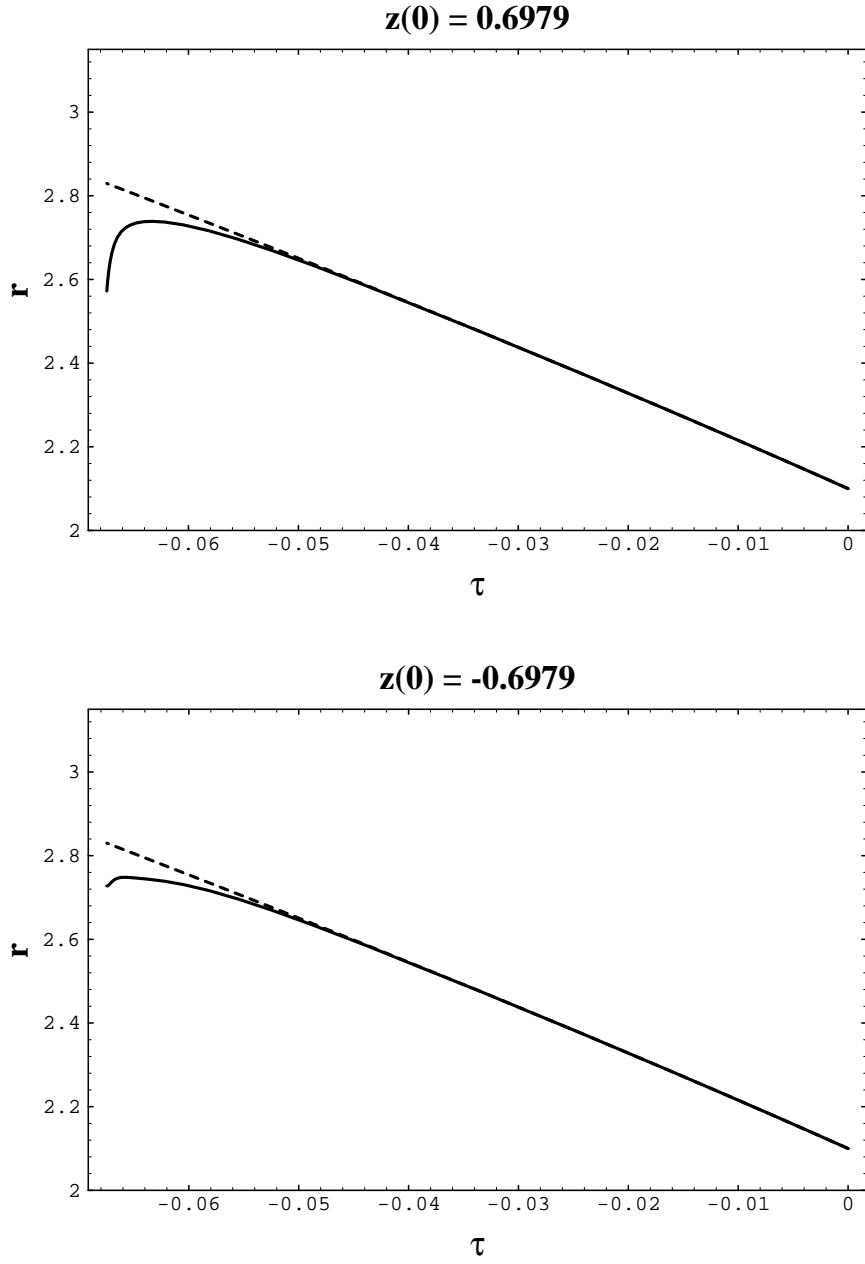


Figure 4: Radius of the dust cloud at two non-polar points

#### 4. Conclusion

In this paper we have started to tackle the problem of matching a dust interior to the Robinson-Trautman exterior. A full solution to this matching problem would shed light on the physical interpretation of Robinson-Trautman spacetimes by recreating the dynamics of dust sources which generate Robinson-Trautman radiation.

Given that any non-trivial Robinson-Trautman solution must be numerically generated in part it is unreasonable to expect to find a matter interior in closed form. At first glance

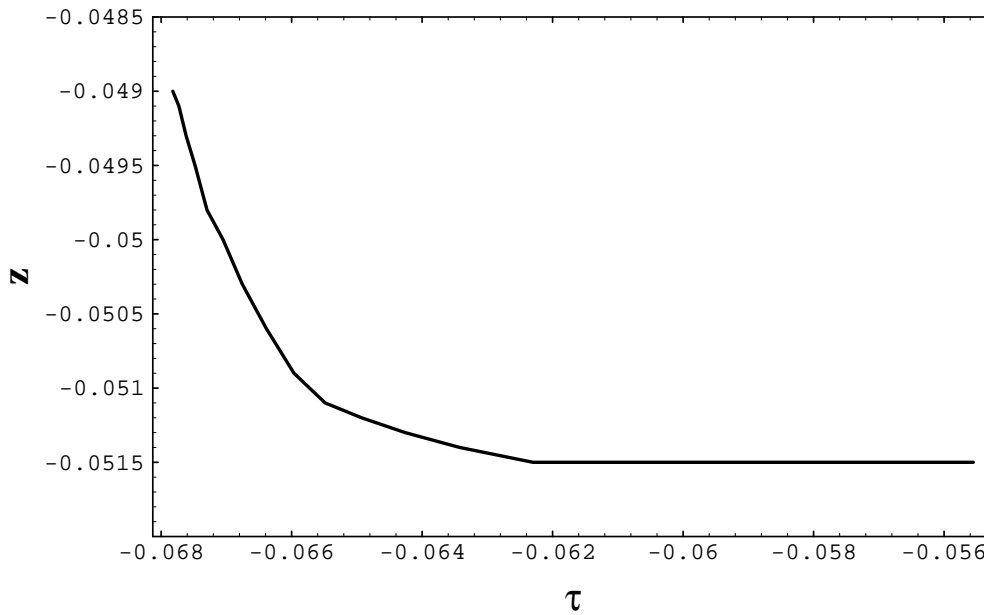


Figure 5: Angular motion of a dust particle near the equator

it would seem that the most physically sensible approach to the problem would be to arrange a forward simulation, in which a dust cloud of appropriate initial configuration is evolved forwards to determine the dynamics of the collapse. Unfortunately such an approach appears to be infeasible. The initial configuration of the dust-cloud determines the dynamics of the vacuum exterior — it gives off radiation — and we have no way of knowing *a priori* what kind of dust clouds generate Robinson-Trautman radiation.

Guided by the fact that the pure Robinson-Trautman solution must settle down to the Schwarzschild solution, we have chosen instead to solve an inverse problem: *Given an Oppenheimer-Snyder final state, what kind of initial dust-cloud could have generated the Robinson-Trautman exterior?* To solve this problem it is necessary to evolve backwards — information now flows inwards — to allow the Robinson-Trautman exterior to determine the shape of the boundary and to provide the boundary conditions which distort the interior away from the Oppenheimer-Snyder dust-ball.

The next stage of our matching program involves evolving the interior backwards, starting with a spatial slice of the Oppenheimer-Snyder dust-ball, using a using a 3+1 numerical algorithm.

## 5. References

1. S J Fletcher and A W C Lun, Bondi-Sachs Metrics and Angular Momentum, in *Proceedings of the Fourth Monash Workshop in General Relativity*, A W C Lun, L C Brewin and E W-M Chow, eds, 1994, Monash University, Melbourne.
2. I Robinson and A Trautman, Some Spherical Gravitational Waves in General Relativity, *Proc Royal Soc Lond* **A265**: 463 (1962).

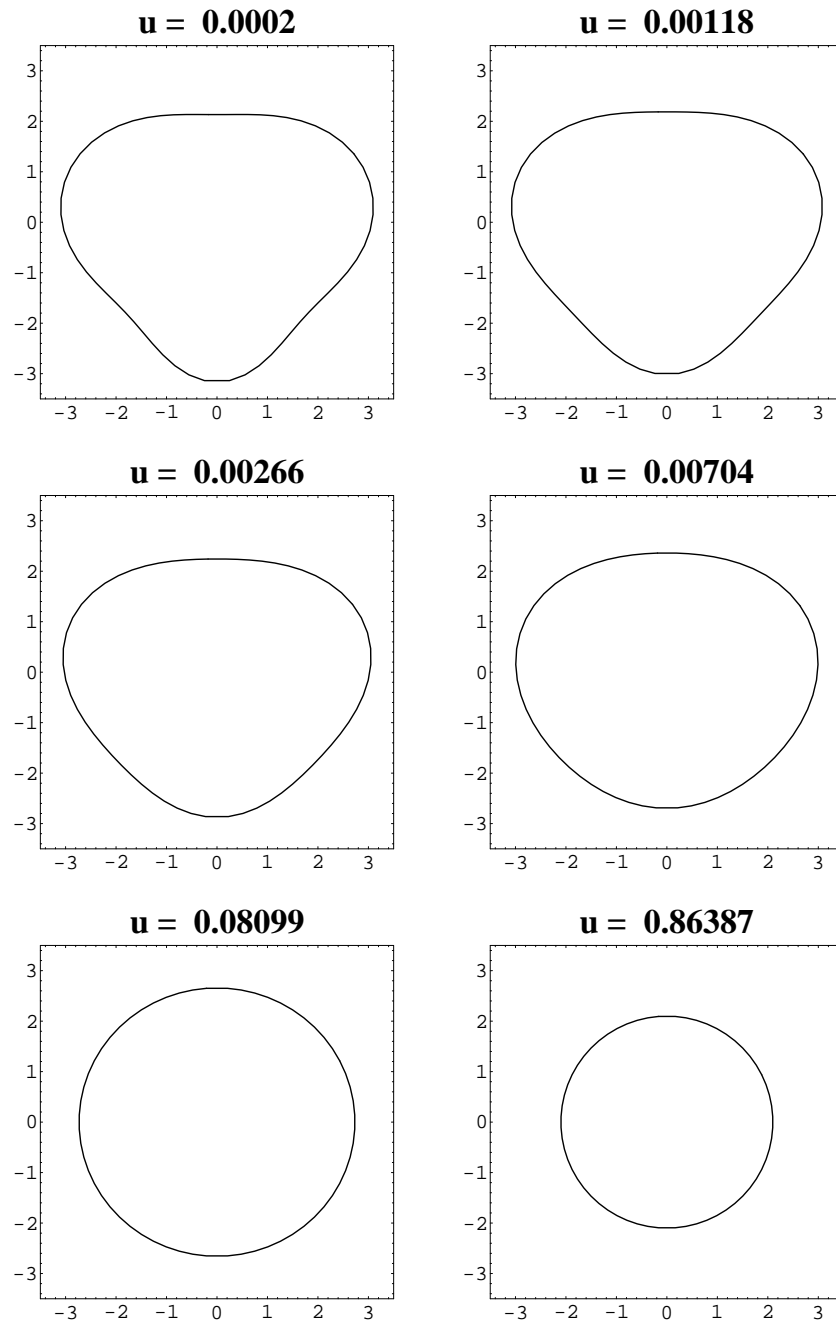


Figure 6: Snapshots of the dust-cloud

3. A W C Lun and E W-M Chow, 'The Role of the Apparent Horizon in Electrovac Robinson-Trautman Spacetimes', in *Confronting the Infinite*, A L Carey, W J Ellis, P A Pearce and A W Thomas, eds, 1995, World Scientific, Singapore.
4. B Lukács, Z Perjés, J Porter and Á Sebastyén, Lyapunov Functional Approach to Radiative Metrics, *General Relativity and Gravitation* **16**: 691-701 (1984).
5. P T Chruściel, Semi-Global Existence and Convergence of Solutions of the Robinson-

- Trautman (2-Dimensional Calabi) Equation, *Commun Math Phys* **137**: 289–313 (1991).
6. K P Tod, Analogues of the Past Horizon in the Robinson-Trautman metrics, *Class Quantum Grav* **6**: 1159 (1989).
  7. D A Prager and A W C Lun, Numerical integration of the axisymmetric Robinson-Trautman equation by a spectral method, to appear in *Jour Aust Math Soc B*.
  8. D Singleton, *Robinson-Trautman Solution of Einstein's Equations*, PhD thesis, Monash University, Melbourne, 1990.
  9. E W-M Chow, *Apparent Horizons in Robinson-Trautman Spacetimes*, PhD thesis, Monash University, Melbourne, 1996.